Seismic anisotropy beneath Central Australia: A record of ancient lithospheric deformation

Caroline M. Eakin[1*], Claire Flashman[1], Shubham Agrawal[1]

1) Research School of Earth Sciences, The Australian National University, 142 Mills Road, Canberra, ACT 2601, Australia

* Corresponding author (caroline.eakin@anu.edu.au)

Highlights

- **KS* splitting presented for the BILBY array in Central Australia
- Splitting pattern shows strong resemblance to the surface geology
- Reflects anisotropy generated by past lithospheric deformation of the continent
- Suggests past tectonic events substantially impacted both crust and lithosphere

Abstract

From 2008-2011 a broadband seismic array (BILBY) spanned the Australian continent from North to South, crossing the suture zone between the North and South Australian cratons, and traversing the Central Australian orogenic belt. Past tectonic events, including orogenies during the Proterozoic and Paleozoic, have left a long-lasting impression on the crustal and Moho structure of this inter-cratonic region. However, the impact of past tectonic activity on the lithosphere has been less clear. Here we present the first shear-wave splitting results for the BILBY array using a combination of *SKS* and *PKS* teleseismic phases to investigate patterns of deformation and seismic anisotropy within the upper mantle beneath central Australia. Null **KS* observations are found to be abundant compared to observations of splitting, as has been widely reported by previous studies, but this appears to be largely due to a coincidental alignment of the inferred anisotropic fast direction with the back-azimuthal range at which most available events occur (140°-160°). Across the central Australian belt the station averaged fast directions tend to orientate ENE-WSW parallel with topographic, gravity, and magnetic trends. Northwards however, the fast directions switch orientation, instead following the NW-SE elongated geometry of the Tennant Creek Inlier, thus delineating a sharp lateral change in the underlying seismic anisotropy. Overall, evidence suggests that the splitting pattern likely reflects anisotropy inherent within the lithosphere generated by past deformational events over 300 million plus years ago, as opposed to the present-day mantle flow in the asthenosphere. While two distinct layers of anisotropy, present in both the asthenosphere and lithosphere, is supported by other evidence, it is not necessarily required by our current dataset. Instead, we can sufficiently model our results with only a single layer of anisotropy, consistent with the expected geometry of azimuthal anisotropy in the lithosphere.

Keywords

Seismic anisotropy; Australia; Lithosphere; Shear-wave splitting; Continental deformation; Suture zone;

1. Introduction

Since the cratonic assembly of the Australian proto-continent during the Precambrian, the region of central Australia has played host to an extensive history of orogenic and deformation cycles, culminating with the Alice Springs Orogeny 300-400 million years ago (Haines et al., 2001; Myers et al., 1996). This history is visibly recorded by pronounced patterns in the landscape and geophysical characterisation of central Australia. At the surface, the geology reflects an alternating pattern of parallel uplifted blocks and sedimentary basins (Figure 1b). Below the surface, gravity surveys have revealed some of the strongest intra-plate and intra-continental gravity anomalies in the world (Bacchin et al., 2008), with a striking east-west trend (Figure 1c). These anomalies reflect a series of crustal uplifts and Moho offsets of 10km or more, indicating crustal features which have remained out of isostatic equilibrium for at least 300 Ma (Aitken, 2010; Aitken et al., 2009b, 2009a; Goleby et al., 1989; Lambeck and Burgess, 1992; Sippl, 2016). In order to maintain such features over time a supporting contribution from the mantle lithosphere is implied (Lambeck, 1986, 1983), as is an expectation that the lithosphere would also accommodate some of the deformation (e.g. Kennett and Iaffaldano, 2013), assuming that there is at least some degree of mechanical coupling between the crust and the mantle (Vauchez et al., 1998). It is difficult to imagine such significant long-lasting deformation of the whole crustal structure without also impacting the lithosphere. However, passive seismic studies as a whole have found little evidence of past deformational cycles within the central Australian lithosphere (e.g. Kennett and Sippl, 2018). While there have been some hints of a layered lithospheric seismic structure including mid-lithospheric discontinuities (Fichtner et al., 2010, 2009; Fishwick and Reading, 2008; Ford et al., 2010; Kennett and Sippl, 2018; Yoshizawa, 2014), sharp lateral transitions in seismic properties have largely so far gone undetected.

Deformation of the mantle, whether in the lithosphere or asthenosphere, is expected to generate seismic anisotropy from the lattice-preferred orientation (LPO) of olivine minerals (Ismaïl and Mainprice, 1998; Nicolas and Christensen, 1987). In the lithosphere this LPO is typically fossilized or frozen-in since the last deformational episode, while in the asthenosphere it represents active present-day mantle flow (Long and Becker, 2010). The relative contributions of this lithospheric versus

asthenospheric anisotropy to the observed signal in continental settings, especially where thick cratonic lithosphere is present, remains unclear (Fouch and Rondenay, 2006; Long and Becker, 2010). In Australia, surface wave studies reveal strong azimuthal anisotropy at the base of the plate aligned with the present-day rapid plate-motion towards the north (Debayle et al., 2005; Debayle and Ricard, 2013; Simons et al., 2002). Conversely, shear wave splitting studies, largely based on sparse continental scale broadband arrays, present an overall lack of coherent splitting that would suggest an isotropic or weakly anisotropic mantle, and show scant evidence for plate motion aligned anisotropy (Chen et al., 2021; Heintz and Kennett, 2006, 2005; Özalaybey and Chen, 1999). In some locations there have been hints of similarity between the shear wave splitting results and the crustal structural fabric, but this has been limited regionally (Bello et al., 2019; Clitheroe and van der Hilst, 1998; Heintz and Kennett, 2005). Heintz and Kennett (2006) proposed a two-layer model in which the lithosphere would contain fossilized anisotropy orientated perpendicular to the asthenospheric flow field, essentially resulting in destructive interference. Recent work analysing patterns of Love-to-Rayleigh scattering has hinted at lateral gradients in seismic anisotropy present within the Australian continental lithosphere, including beneath central Australia (Eakin, 2021).

In this study we provide the first results of shear wave splitting from the BILBY array to analyse upper mantle seismic anisotropy beneath central Australia. The geometry of the array, encompassing a relatively dense 1000 km long transect from north to south, crosses the suture zone between the North and South Australian Cratons including the prominent E-W parallel gravity anomalies and associated uplifted tectonic blocks (Figure 1). Such a linear geometry allows us to closely examine and pin-point any lateral variations in seismic anisotropy across the continent, in particular in relation to any potential changes in lithospheric properties associated with past tectonic events.

2. Tectonic Setting

The BILBY array (as shown in Figure 1) spans central Australia from South to North passing through numerous geological provinces of mostly Archean to Proterozoic age. A detailed description of the various geological units underlying the BILBY array can

be found in Sippl, (2016). Here we provide a brief tectonic summary of the key events and primary features of the region.

The three main crustal components of Proterozoic Australia; the North, South, and West Australian Cratons are thought to have been in existence since ~1.8Ga and assembled together during Rodinia by 1.3-1.1Ga to form the proto-Australia continent (Betts and Giles, 2006; Myers et al., 1996). The South Australian Craton formed as an amalgamation of the proto-Gawler and proto-Curnamona cratons, while the North Australian Craton was created from the accretion of multiple crustal fragments. The Tennant Creek Inlier at the northern end of the BILBY profile represents one particular suture between such crustal fragments (Myers et al., 1996; Zhao et al., 2002). From the Mesoproterozoic onwards, these suture zones, the boundaries along which crustal fragments had collided and fused, would form lines of weakness controlling the geometry of subsequent continental deformation.

Following continental assembly, from 830-750 Ma large scale subsidence and sedimentation occurred over much of central Australia creating the Centralian Superbasin (Walter et al., 1995). Break-up of Rodinia followed at ~750 Ma initiating a NE-SW compressive regime across the continent (Myers et al., 1996). Two intra-continental deformational events- the Petermann Orogeny (570-530 Ma) and the Alice Springs Orogeny (450-300 Ma)- reactivated old structures to subdivide the Centralian Superbasin into several smaller basins including the Amadeus, Ngalia, and Georgina basins (Sippl, 2016). During the same events the Musgrave and Arunta blocks were uplifted, with crustal shortening accommodated along E-W striking crustal-scale faults, such as the Redbank Shear Zone which bounds the Arunta block to the south. As a result the crust is significantly thinner beneath the Musgrave and Arunta blocks with respective Moho offsets of around 10 km and 20 km (Aitken, 2010; Goleby et al., 1989; Lambeck and Burgess, 1992; Sippl, 2016). Higher density mantle at depths equivalent to the lower crust beneath these uplifted blocks is thought to produce the prominent E-W elongated central Australian gravity anomalies with amplitudes of ~1500 $\mu m/s^2$, as seen in Figure 1 (Bacchin, 2010). Since the end of the Alice Springs Orogeny at 300 Ma central Australia has largely remained tectonically quiescent.

3. Methods and Data

3.1 Detection of seismic anisotropy from shear wave splitting

When a shear wave enters an anisotropic medium it becomes polarised into two quasi-*S* waves, a fast and a slow component, which are effectively orthogonal. Due to the difference in wave speed, on the seismogram the fast and slow arrivals accumulate a delay time (∂t) between them that reflects the strength of anisotropy and/or the length of the raypath through the anisotropic material. In shear wave splitting analyses, the aim is to measure this delay time, as well as the orientation of the fast direction (Φ) to infer the geometry of the anisotropy within the medium. Teleseismic refracted phases, such as SKS, that have travelled through the outer core, are particularly useful as they isolate the anisotropic signature of the mantle beneath the receiver (i.e. directly beneath the seismic station). Any anisotropy in the mantle beneath the seismic source is removed when the down-going *S*-wave converts to a *P*-wave at the core-mantle boundary. Similarly when the *P*-wave reconverts to a *S*-wave at the core-mantle boundary on the upward leg, the initial polarisation of the *S*-wave is aligned to the source-receiver plane (i.e. the back-azimuth).

Throughout the mantle, the primary source region of seismic anisotropy, and therefore the primary source of SKS splitting, is thought to originate in the upper mantle from the lattice preferred orientation (LPO) of olivine (Nicolas and Christensen, 1987). When the upper mantle undergoes strain or deformation (i.e. mantle flow) via dislocation creep, the dominant upper mantle mineral olivine undergoes a crystallographic rotation relative to the direction of shear (e.g. Karato et al., 2008). The preferential orientation of olivine crystallographic axes results in an effective bulk anisotropy that is detectable and measurable by techniques such as shear wave splitting. This crystallographic preferred orientation of olivine may reflect either present or past mantle deformation, depending on whether mantle flow is presently active and therefore continually developing LPO (e.g. in the asthenosphere), or deformation has since ceased, effectively 'freezing' or 'fossilizing' the last LPO-fabric to have developed (e.g. in the lithosphere) (Silver and Chan, 1991). Other potential anisotropic contributions include the lowermost mantle in the D" layer

(Kendall and Silver, 1996), or crustal anisotropy due to the shape preferred orientation (SPO) of fluid filled cracks (e.g. Crampin, 1994), or ductile deformation of the lower crust (e.g. Rabbel and Mooney, 1996). Such contributions are usually minor in comparison to the upper mantle due to their relatively limited spatial extent and small path lengths for steeply incident SKS phases (Long and Becker, 2010).

3.2 Stations and events

In this study **KS* (*SKS* and *PKS*) shear wave splitting analyses were conducted for the 25 stations from the BILBY array (Rawlinson and Kennett, 2008), as well as three co-located permanent stations (II.WRAB, AU.AS31, AU.MULG). The BILBY array was deployed on a north-south transect through central Australia from 2008 until 2011 with an average station spacing of ~85km (Figure 1). Due to the harsh operating conditions of the Australian continental interior, several stations at the north-eastern and southern extremities of the array suffered significant recording outages, including sites BL: 01-02, 04-05, 21-23, 25, and therefore had a reduction in data available for study. The three permanent stations had significantly longer operating periods with WRAB operational since 1994, AS31 since 2005, and MULG since 2013. The addition of these 3 permanent stations provides useful reference points along the array, with WRAB located in the north near Tennant Creek, AS31 in the central section at Alice Springs, and MULG in the south within the Gawler Craton.

For event selection, earthquakes were restricted to magnitudes greater than 6.0 to ensure significantly strong signal for **KS* splitting analysis. The epicentral distance between source and receiver was chosen to be between 90°-130° for *SKS* and 130°-150° for *PKS*, to generate near vertical incidence angles (<10°) and to avoid interaction with other phase arrivals.

Over the timespan of the BILBY array 105 suitable events occurred, resulting in 1300 individual event recordings analysed across the 25 station array (Figure 2a). While events occurred in a range of back-azimuthal quadrants they are most plentiful from South America in the SSE direction, with ~35% of all events concentrated in the 140°-160° back-azimuthal range. A similar spatial distribution of events is retrieved for the three permanent stations (Figure 2b).

3.3 Shear-wave splitting processing and methodology

Shear wave splitting analyses were performed for all stations using the SplitLab software package (Wüstefeld et al., 2008). Within this application, for the purposes of quality control, we compared the shear wave splitting parameters (fast direction Φ, delay time ∂t) found by two independent methods; the rotation correlation (RC) and minimum energy (SC) methods.

The RC method (Bowman and Ando, 1987) systematically rotates the quasi-shear waves to determine the fast direction (Φ_{RC}) and delay time (δt_{RC}) for which the cross-correlation coefficient is greatest. Results from the RC method are known to deviate significantly from true values when the initial polarisation approaches the same orientation as the fast or slow axis of anisotropy (i.e. predicted null directions) (Wüstefeld and Bokelmann, 2007). In such cases, δt_{RC} values diminish to zero, and Φ_{RC} can vary up to 45 degrees away from the true value. The SC method (Silver and Chan, 1991) is thought to be more stable across a wider range of initial polarisations (i.e. back-azimuths for **KS*) but is susceptible to similar deviations at moderate signal-to-noise ratios (Eakin et al., 2019). The SC method selects the combination of Φ_{SC} and δt_{SC} for which the energy on the transverse component of the wave is minimised. It is most useful for *SKS* splitting where the orientation of the initial polarisation is known. In following sections, the results from the SC method are presented for further discussion, unless otherwise stated.

Following our previous work (Eakin et al., 2019, 2015) all splitting measurements were visually inspected and subject to strict quality control, with both quantitative and qualitative conditions applied. Firstly, to increase the signal-to-noise ratio (SNR), the data were bandpass filtered using a Butterworth filter with a frequency band from 0.04Hz to 0.125Hz. High quality seismograms identified by visual inspection, and SNR values >5, were then selected for further analysis. Quantitative conditions applied for a split result (i.e. non-null) included errors less than 1 second in ∂t and less than 22.5° in Φ at the 95% confidence level, in addition to agreement between the RC and SC methods within $|\Phi| < 22.5$ °, and $\partial t_{RC}/\partial t_{SC} > 0.7$ following (Wüstefeld and Bokelmann, 2007). Qualitative measures of splitting included visual identification of a clearly visible shear wave pulse above the noise and of similar shape on both the

estimated fast and slow components, elliptical initial particle motion which upon correction becomes linearized towards the back-azimuth, and minimal energy on the corrected transverse component. An example of a well-constrained splitting measurement with these characteristics is shown in Figure S1.

Null results, which suggest the **KS* phase has not undergone any splitting can provide useful additional information to help constrain the orientation of anisotropy. A null result was defined as having (i) linear initial particle motion along the direction of the back-azimuth, (ii) a clearly visible **KS* pulse on the uncorrected radial component, (iii) little to no **KS* energy on the uncorrected transverse component. Null measurements tend to also display zero (or near-zero) apparent delay times for the RC method (δt_{RC}), in contrast to larger predicted delay times for the SC method (δt_{SC}), as utilised by (Wüstefeld and Bokelmann, 2007). An example of a well-constrained null measurement can be found in Figure S2.

Lastly, during the visual inspection process, observations were noted of any systematic offsets between the backazimuth and uncorrected particle motion (in particular null measurements with linearized motion). This is often an indication that the seismic station is misaligned with north, but can be easily corrected (e.g. Figure 3 of Eakin et al., 2018). If the station is correctly orientated then the initial polarisation (determined from the orientation of the uncorrected particle motion) should match the event backazimuth. When the station is not orientated correctly then the angle between the initial polarisation and the back-azimuth is measured for a range of events, and the average is taken as the station misalignment value. We discovered that two stations (BL24 and BL08) required such corrections. BL24 was rotated 8° clockwise from north, while BL08 had three separate values applied (0°, i.e. no correction, up until 26/02/2010; 340° clockwise during 27/02/2010-25/03/2010; and 16° clockwise after 26/03/2010 until final operation on 15/02/2011). Furthermore, a small correction of 7° was applied to permanent station MULG, while for station WRAB a correction of -64° (anticlockwise from north) was necessary from 09/2009 onwards.

4. **KS* Splitting Results

Our **KS* splitting analysis for BILBY stations returned 155 measurements from 53 unique events (Figures 3-5, Table S1). Of these measurements 16% were splits, i.e. non-null measurements (13 *SKS* splits and 12 *PKS* splits), while the remaining 84% were null (88 *SKS* null and 42 *PKS* null). The 25 splits were generated from 23 different events. On average each station had 6 results, with 1 split and 5 nulls. A small number of results is typical for such temporary deployments (e.g. Eakin et al., 2019, 2015, 2010). Several stations produced no results (BL: 18, 19, 21, 25) due to poor data quality. Station BL24 had the highest number of results, 16, of which 15 were null. Stations BL14 and BL15 had the highest number of non-null measurements each with four.

Although there are on average only a handful of results at each BILBY station, the characteristics of the splitting are broadly similar from station to station, and with nearby permanent stations (Figure 3). For comparison, station AS31 recorded 16 splits (mean Φ: 72°, mean ∂t: 0.9s) and 15 nulls. Station MULG had fairly similar splitting parameters with 14 split results (mean Φ: 75°, mean ∂t: 1.3s) and 8 nulls. Station WRAB differed with 6 splits (mean Φ: -17°, mean ∂t: 0.8s) and 35 nulls. However, when directly comparing the number of results over the same two-year timespan of BILBY, AS31 produced 1 split (Φ: 78°, ∂t: 1.0s) and 3 nulls, while WRAB produced 1 split (Φ: -14°, ∂t: 0.6s) and 6 nulls. This smaller number of results is consistent with the average number of measurements per station we found for the BILBY array, indicating similarity in results between the permanent and temporary stations over the same time period. Additionally, the splitting parameters retrieved at permanent stations from one split measurement during the BILBY time period are comparable to the mean values for the whole time period for those stations. This suggests that even though the number of split measurements at individual BILBY stations may be small, it is not unreasonable to assume that they will be broadly reflective of a longer term pattern, particularly when there is consistency from station to station.

In Figure 3a we plot the average splitting parameters for each station in map view and in Figure 4 as a function of latitude. Below 22°S, stations show consistent ENE-WSW fast directions (Φ: 44°-83°) throughout the central orogenic belt, similar to the E-W trending geological terranes and elongated gravity anomalies.

North of the Arunta block (above 22°S), the fast directions are more variable but largely switch to either SE-NW or SSE-NNW orientations. For northernmost stations BL06, BL07, and WRAB, there is a degree of variability between stations but overall the fast directions are similar to the SE-NW strike of the Tennant Creek Inlier on which the stations reside. To the east of these stations, over the Georgina Basin, there are two stations which recorded splitting. The fast direction between these two stations however is rather different, from 3° at BL01 versus 109° at BL03, potentially indicating changes in the anisotropic structure underneath. Across the array there are no obvious spatial trends in the station averaged delay times, with values ranging from 0.75 to 1.50 seconds (Figure 4).

For both BILBY and permanent stations, with the exception of MULG, null results are considerably more common than split results at each station. Figure 5 shows that the backazimuthal distribution of both null and split results largely reflects the backazimuthal availability of events, which is dominated by events in the 140°-160° back-azimuth band. If one compares this 140°-160° band, where most events originate, with the station averaged fast directions, as in Figure 4, it can be seen that there is considerable overlap. This suggests that the backazimuth of the majority of events happens to be aligned with the inferred fast/slow axes of anisotropy beneath most stations, which likely accounts for why nulls are more prevalent than splits across BILBY stations.

Given the relatively small number of results at each BILBY station, it is not possible to further investigate any back-azimuthal dependency of results. The three permanent stations do however display clear variation and a 90° periodicity in the splitting parameters with back-azimuth (Figure 6). Most notably, at all 3 stations, there is a distinct rotation of the fast direction with back-azimuth that follows a 45° slope, i.e. Φ = backazimuth ±45°, as represented by the solid black line in Figure 6. This pattern is consistent with a known systematic error in splitting measurements, as previously modelled in synthetic tests (Monteiller and Chevrot, 2010; Vecsey et al., 2008; Wüstefeld and Bokelmann, 2007) and observed in real datasets (Eakin et al., 2019). As would be expected the pattern is present for both SC and RC methods but is most pronounced for the rotation correlation (RC) method (Figure S4). Therefore, despite significant variability in results with backazimuth, the splitting

results at our three permanent stations are still consistent within error to the predictions of a single layer of anisotropy characterised by the station average Φ and ∂t parameters.

5. Discussion

Although the overall properties of the **KS* splitting results along the BILBY profile are found to be consistent with a simple single uniform layer of anisotropy, multiple layers of anisotropy could arguably be expected in continental settings with thick continental lithosphere (Conrad et al., 2007; Fouch and Rondenay, 2006). In central Australia, studies of azimuthal anisotropy from surface wave tomography provide supporting evidence for such a view (Debayle et al., 2016, 2005; Debayle and Ricard, 2013; Simons and van der Hilst, 2003), an example of which is shown in Figure 7. In general spatially heterogeneous anisotropy is imaged in the upper 100 km, interpreted as lithospheric anisotropy, while between depths of 150-250 km strong azimuthal anisotropy is aligned with the north-northeast plate motion of Australia (as inferred from global geodetic plate motion models such as Kreemer et al., 2014). Likewise studies of radial anisotropy find strong radial anisotropy ($V_{SH} > V_{SV}$) beneath Australia at similar depths (Yoshizawa, 2014; Yoshizawa and Kennett, 2015). Both sets of observations have long been interpreted as the expression of rapid plate motion exerting significant horizontal shear on the underlying asthenosphere beneath Australia (e.g. Debayle et al., 2005).

It is clear that our results from BILBY, as well as other shear splitting studies across Australia (Bello et al., 2019; Chen et al., 2021; Clitheroe and van der Hilst, 1998; Heintz and Kennett, 2006, 2005; Özalaybey and Chen, 1999), do not primarily reflect this anisotropic layer of asthenospheric N-S aligned shear. Interestingly, however, our station averaged splitting results do show a striking correspondence with azimuthal anisotropy imaged within the lithosphere below the BILBY profile (Figure 7), suggesting that to first order the splitting measurements are primarily indicative of the underlying frozen-in lithospheric anisotropy. This assertion is further supported by qualitative agreement between the station averaged fast directions and surface features, in particular the E-W orientation of the elongated gravity anomalies and associated major geological terranes (Musgrave-Amadeus-Arunta provinces), as well

as the change to the NW-SE orientation of the Davenport Ranges and Tennant Creek Inlier (Figure 3).

Given that asthenospheric flow is expected to be fairly uniform across the region, the change in splitting parameters at 22°S strongly suggests a sudden change in lithospheric anisotropy that reflects the spatial extent of past continental deformation episodes. Furthermore, the change in azimuthal anisotropy fast direction imaged within the shallow lithosphere (Figure 7) is shown to be gradual at ~ 50 km depth, i.e., changing colour and orientation from south to north from yellowish beige (~70°) to brown (~40°) to purple (~0°) to blue (120°-140°). The change in the splitting however is much sharper, from continuously beige/brown stations (i.e. triangles) up until BL12 to a sudden switch to blue/purple at BL10. It is likely that the surface wave tomography (Debayle et al., 2016) has smoothed this anisotropic change to produce a gradual gradient, whereas the receiver-based shear wave splitting reveals a comparatively sharp boundary in anisotropic properties that spatially correlates with the surface geology.

While it is understandable that the lithosphere may preserve anisotropy that is detectable by shear-wave splitting, it is surprising that a substantial contribution from the asthenosphere is not more readily apparent given the relative strength of azimuthal anisotropy at asthenospheric depths as imaged by surface waves (e.g. Figure 7). We propose two possible solutions to this. The first possibility is that in the presence of an anisotropic medium of relatively uniform strength but with a fast axis orientation that varies considerably with depth, the **KS* splitting measurements are more biased towards the upper portions of the anisotropic medium than the deeper. Modelling of such vertically varying anisotropy and synthetic seismograms by Saltzer et al., (2000) supports such an idea. In their study calculation of the Fréchet sensitivity kernels demonstrated that splitting measurements made at low frequencies typical of *SKS* splitting (~0.1 Hz) would produce apparent fast directions that deviated from the true average of the medium. Instead the splitting retrieved would be weighted towards the orientation of the anisotropy in the upper section of the model, in particular with highest sensitivity at around one-third of the depth. This follows shear-wave splitting observations across several stable continents in which the measured fast directions show a high degree of similarity with surface geology (Aragon et al., 2017; Bastow et

al., 2007; Helffrich et al., 1994; Liu et al., 2020; Silver and Chan, 1988; Silver, 1996; Silver et al., 2001). If such a scenario is true, whereby **KS* splitting measurements are biased towards the upper part of the anisotropic mantle, then this suggests that shear-wave splitting is a currently under-utilised tool for studying lithospheric anisotropy and past-deformation across Australia.

Alternatively, the second possibility is to attempt to fit our results with a two-layer model of anisotropy, in which the lower layer represents the asthenosphere and the upper layer the lithosphere. Due to the limitations of the present dataset however, considering all two-layer possibilities and searching for the best-fit model proves unfruitful (Figure S5). Such modelling results are either poorly constrained due to a small number of data-points (e.g. for station WRAB), or return the two-layer solutions that are most similar to the one-layer solution (stations AS31 and MULG). Instead, we consider it more informative to assess whether our results are consistent with the two-layers of anisotropy as would be predicted from current surface-wave azimuthal anisotropy models (e.g. Figure 7).

In Figure 8a-f we show the predicted splitting parameters for such two-layer models following Silver and Savage (1994) and compare with our results from the three permanent stations included in our study. Beneath each station we model the orientation of the fast axis (dotted turquoise line) based on how the properties of the azimuthal anisotropy (blue line) vary with depth (Figure 8g-i). For all stations the azimuthal anisotropy profiles generally show a swing in fast directions above and below ~125 km depth, consistent with a difference between lithospheric and asthenospheric anisotropy. In order to provide the greatest contrast, the end-member fast-direction values in the upper 50-100 km are chosen for the lithospheric layer, and in the depth range 150-250 km for the asthenospheric layer. For station WRAB the average value between 150-250 km depth is chosen instead to smooth out the small fluctuations. For each station we consider five cases with varying delay time contributions. In the first case, the delay time attributable to each layer is equal (0.5 seconds each). In the second and third cases, the delay time difference between the two layers equates to 0.5 seconds (i.e. model 1: ∂t_{upper} =1.0s, ∂t_{lower} = 0.5s; model 2: ∂t_{upper} =0.5s, ∂t_{lower} = 1.0s). Lastly in the fourth and fifth cases, the delay time difference between the two layers is 1 second (i.e. model 1: ∂t_{upper} =1.5s, ∂t_{lower} =

0.5s; model 2: ∂t_{upper} =0.5s, ∂t_{lower} = 1.5s). If the delay times are increased any further then the average value over the back-azimuthal range 0°-60° exceeds the magnitude of the observed apparent delay times (~1s).

As is expected, the two-layer models do not reproduce the 45° slope in fast direction with backazimuth, which is the fundamental variation present within the dataset. That said, some models are more consistent with the splitting data than others. For stations MULG and AS31, models in which the upper layer has a larger delay time than the lower layer (purple and red dotted curves in Figure 8) provide more overlap with the data (considering the error bounds) compared to other models. This would suggest anisotropy in the lithosphere dominates over anisotropy within the asthenosphere in terms of contribution to the splitting signal. In contrast, for station WRAB near Tennant Creek, models in which the lower layer (i.e. asthenosphere) has the larger delay time (yellow and green dotted lines) appear to agree with the data better. This is somewhat consistent with the azimuthal anisotropy profile shown in Figure 7, in which the anisotropy is strongest in the asthenosphere beneath WRAB compared to the other stations, however it is also strongest in the lithosphere beneath WRAB also.

While the two-layer models do not provide an overly convincing fit to the data, and certainly do not appear to be required by our results over one-layer, we do not suggest that multiple layers of anisotropy should be disregarded entirely. It is possible that any variation in splitting parameters generated by a two-layer (or multiple layer) scenario is simply overwhelmed by the systematic error that generates the 45° slope in Φ, as described by Wüstefeld and Bokelmann, (2007) and Eakin et al., (2019). Synthetic tests which investigate the expected patterns in shear-wave splitting for a multi-layer system, and that include this systematic error in observations have yet to be explored. At present, it is therefore difficult to identify or constrain any influence of multiple layers on our splitting dataset, but studies of azimuthal anisotropy from surface wave studies would certainly suggest this to be the case. Our results are therefore not inconsistent with two layers of anisotropy, one in the lithosphere, and one in the asthenosphere, but we cannot claim that two-layers are necessary to explain our data alone.

Overall considering the two proposals put forward: shear wave splitting biased to the shallower structure, or a two-layer model, both would suggest significant anisotropy frozen-in within the lithosphere (Figure 9). This implies lithospheric anisotropy that has been preserved for at least 300 million years since the end of the Alice Springs Orogeny, the last deformation event to occur in central Australia. The consistent ENE-WSW splitting fast directions for stations below 22°S, suggest a uniform compressive regime existed at some stage over much of the continent. If dry olivine LPO fabrics such as A-type or D-type are assumed, which are believed to be true of the lithosphere (Karato et al., 2008), then maximum horizontal compression in the general N-S direction would be inferred, in order to generate deformation and anisotropy that is orientated E-W. Considering the typical magnitude of our observed delay times, those on order of 1 second would equate to ~115 km thick layer of anisotropy, if 4% anisotropy typical of olivine aggregates is assumed (Silver and Chan, 1988). This would suggest than anisotropy within the lithosphere is preserved not just within the shallowest upper mantle but throughout a substantial portion of the lithosphere to at least 100-150 km deep. The strength of the anisotropy may however vary within the lithosphere (e.g. Figure 7), in which case weaker anisotropy would require an even thicker layer in order to generate the same delay times.

6. Conclusions

Shear wave splitting from stations along the BILBY profile have revealed anisotropic fast directions parallel to the crustal tectonic fabric with substantial (~0.75-1.5 s) accumulated delay times. Such a relationship strongly suggests that Australia's deformational history is recorded not just in the crustal structures, but also throughout the lithosphere as frozen anisotropy. This anisotropy must have been preserved for hundreds of millions of years, considering the timing of the suture between the North and South Australian Cratons (~1.3Ga) and the date of the last major orogenic event (~450-300 Ma). Even with limited event availability at temporary deployments such as BILBY, relative changes in the splitting parameters retrieved between adjacent sites offer an insight into sharp lateral changes in lithospheric anisotropy at depth, as well as the spatial extent of coherent deformation.

While a surplus of null measurements, often inferred as apparent isotropy (i.e. lacking seismic anisotropy), has long been noted for Australia (e.g. Heintz and Kennett, 2006), we find that this appears to be consequence of the vast majority of the suitable events for **KS* splitting occurring at a backazimuth that is parallel to the inferred fast/slow axis of anisotropy in central Australia. Whether this holds true for the rest of the continent remains to be further investigated, but based on our findings we make two suggestions for the future. Firstly, we find that the addition of *PKS* phases are beneficial for shear-wave splitting studies in the Australian setting, as compared to *SKS* they provide several suitable events at a second backazimuth (*PKS* mostly occur ~90° versus ~150° for *SKS*). Secondly, it is often worth re-examining shear-wave splitting at long running permanent stations that have a decade of more data, as these can reveal complexities in the anisotropic structure (e.g. Eakin and Long, 2013) or systematic errors in the measurements (e.g. Eakin et al., 2019) that are not otherwise detectable with only a year or two deployment. Having a backbone of permanent sites across the continent as reference stations is critical in this respect, allowing for a better understanding of the anisotropic structure at depth.

Data Availability

The BILBY seismic array (network code: 6F; https://doi.org/10.7914/SN/6F_2008) operated from 2008-2011. The seismic data from this deployment is publicly accessible through the AusPass archive (http://auspass.edu.au/) hosted at the Research School of Earth Sciences, Australian National University. Seismic data for the three permanent stations included in this study (WRAB, AS31, and MULG) come from the Australian National Seismograph Network (network code: AU, http://www.fdsn.org/networks/detail/AU/) and the Global Seismograph Network (network code: II; https://doi.org/10.7914/SN/II). Waveforms and meta-data for these two networks were accessed through the IRIS Data Management Center (https://ds.iris.edu/ds/nodes/dmc/). A table of all shear wave splitting measurements made during this study can be found in the supporting information (Table S1).

Acknowledgements

This work was supported by an Australian Research Council Discovery Early Career Researcher Award (DE190100062) and The Australian National University.

514 Deployment of the BILBY array was supported by ARC Discovery Project
515 (DP0662984). We would like to pay acknowledgment to the traditional custodians of
516 the land on which the BILBY stations were deployed, as well as thank RSES staff at
517 ANU who conducted the fieldwork for BILBY. Constructive comments from two
518 anonymous reviewers improved the manuscript. Splitting measurements were
519 processed using SplitLab version 1.2 updated by Robert Porritt
520 (https://robporritt.wordpress.com/software/). Figures were made with the aid of
521 Generic Mapping tools (Wessel et al., 2013), with a scientific color map from
522 Crameri et al., (2020) utilized in Figure 7. Australian geophysical datasets were
523 accessed via https://portal.ga.gov.au/persona/gadds.

Figures

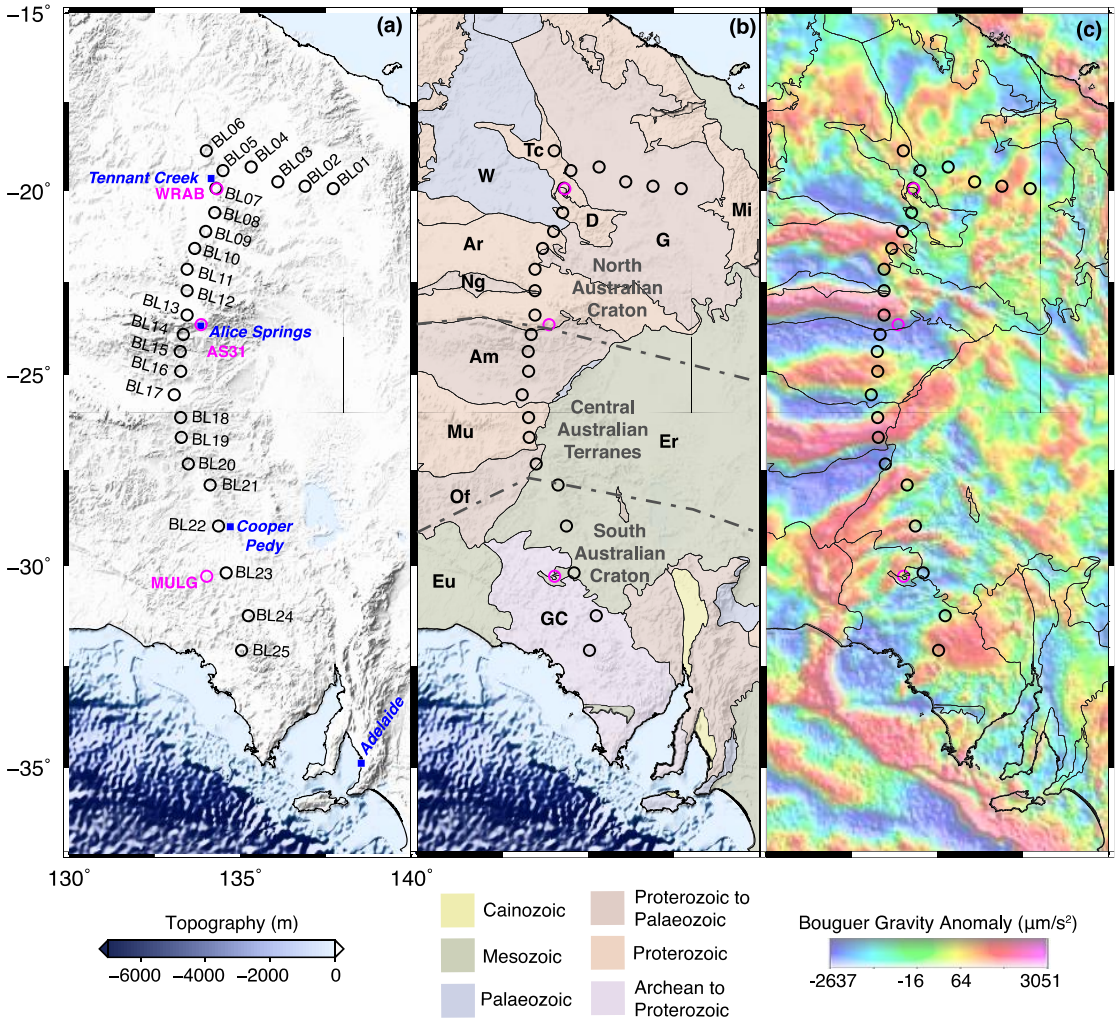
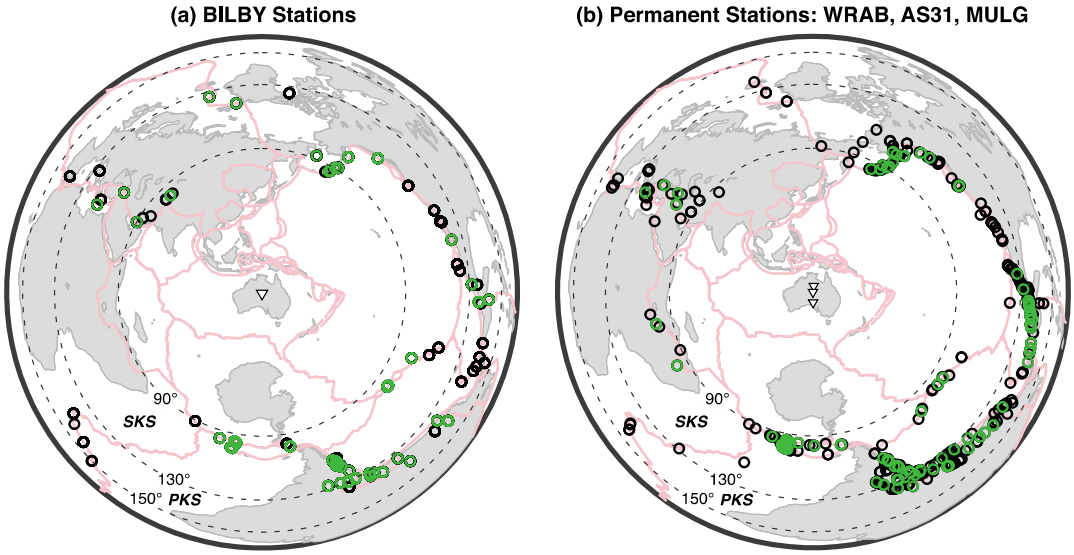


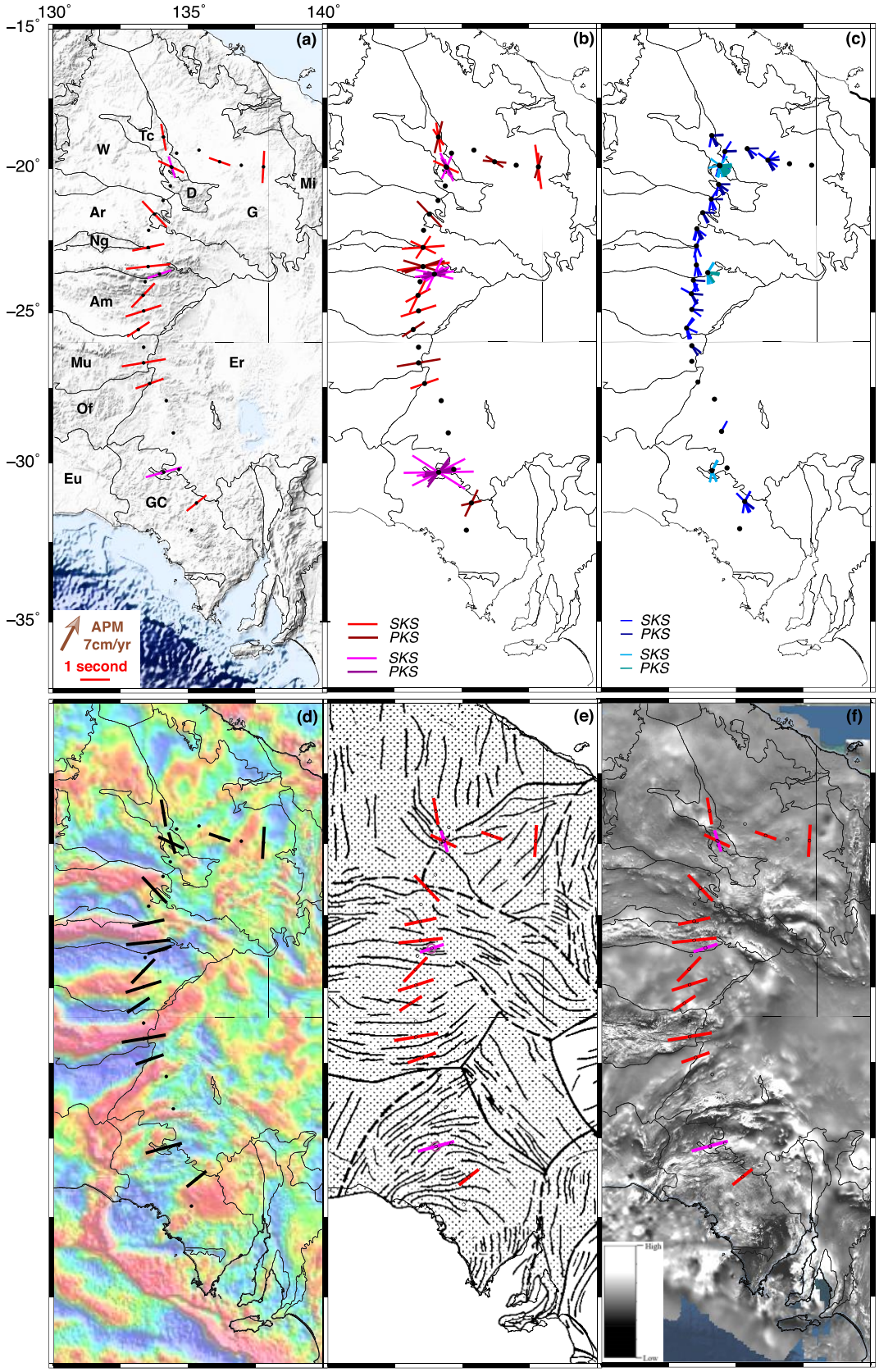
Figure 1. Regional overview of central Australia showing location of the BILBY seismic array (black circles) and three permanent seismic stations (magenta circles) used in this study. The three panels show (a) topography (Amante and Eakins, 2009), (b) Australian geological regions (Blake and Kilgour, 1998), and (c) national gravity anomaly grid (Bacchin, 2010) for the study region. Abbreviations for geological provinces in (b) are as follows: Am – Amadeus Basin, Ar – Arunta Block, D – Davenport Province, Er – Eromanga Basin, Eu – Eucla Basin, G - Georgina Basin, GC – Gawler Craton, Mi – Mount Isa Block, Mu – Musgrave Block, Ng – Ngalia Basin, Of – Officer Basin, Tc – Tennant Creek Block, W – Wiso Basin.



536

537 **Figure 2**. Distribution of events utilised in this study for BILBY stations (a) and
538 permanent stations (b). Those that yielded a result, either split or null, are indicated by
539 green circles, and those that did not as black circles. The seismic arrays are
540 represented by the inverted white triangles. Epicentral distance ranges optimal for
541 *SKS* (90°-130°) and *PKS* (130°-150°) splitting analyses are indicated by dashed black
542 lines. Plate boundaries from (Bird, 2003) shown in pink.

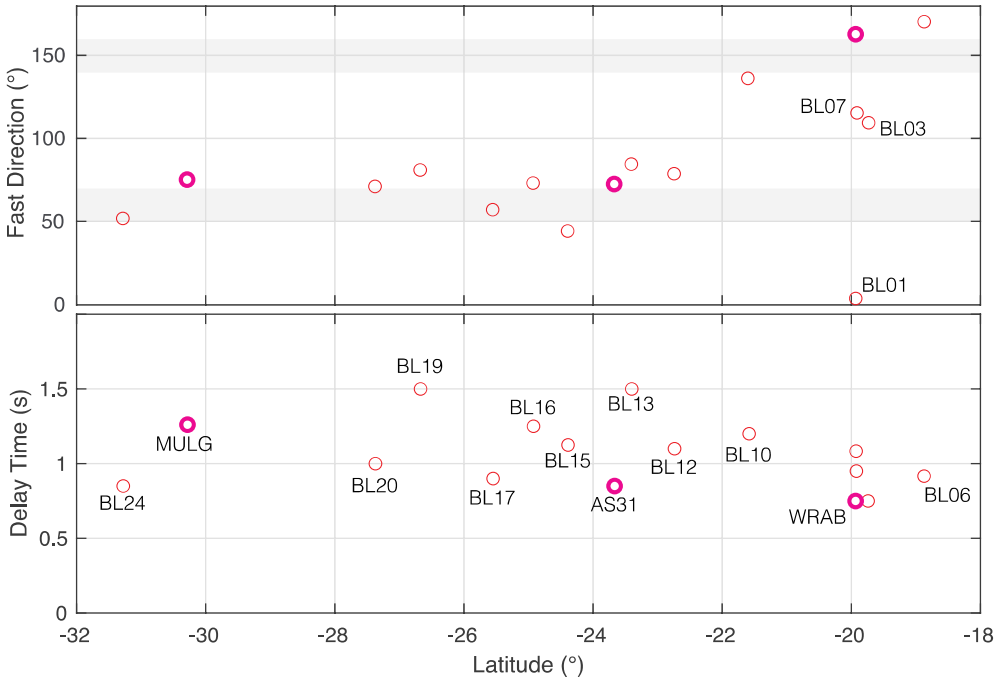
543



544

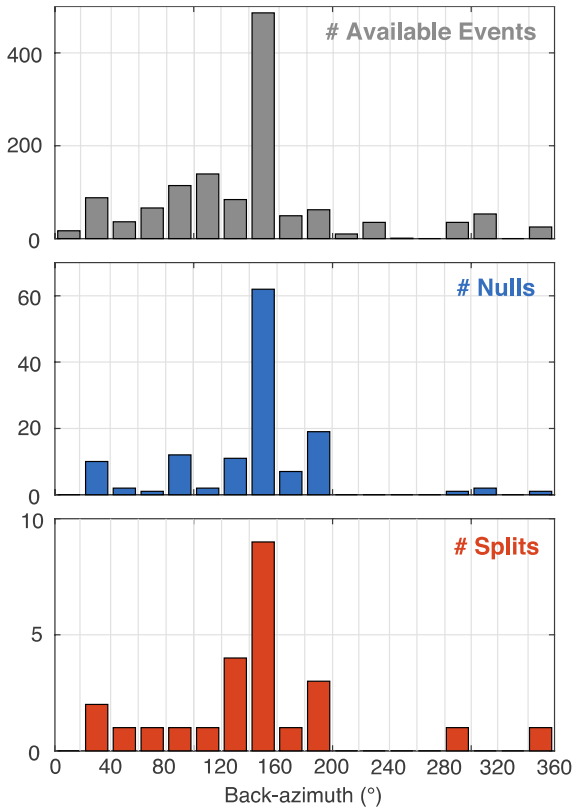
545 **Figure 3**. Map of averaged (a), individual (b) shear wave splitting parameters for each
546 station. The orientation of the coloured bars represent the measured fast directions (Φ).

The length of the bars indicate the corresponding delay time (δt), according to the 1 second scale shown in the legend. Splitting at BILBY stations is represented by red colours and at permanent stations by purple/magenta colours. Geological provinces are outlined in black, with abbreviations, same as Figure 1. The absolute plate motion (APM) beneath central Australia (Kreemer et al., 2014) is indicated by the brown arrow shown in the lower left of figure (a). In (c), individual null measurements are plotted, with each coloured tick pointing in the direction of the event back-azimuth for which the null was observed. Nulls at BILBY stations are shown with blue coloured ticks, and at permanent stations with green/cyan shades. In the lower panel, station averaged splitting parameters from (a) are compared against different geophysical datasets, including (d) gravity anomalies (same as figure 1), (e) inferred gravity trends from Wellman (1976), and (f) total magnetic intensity (Djomani Poudjom et al., 2019).



561
562 **Figure 4**. Station averaged splitting parameters (fast direction and delay time) versus
563 latitude of seismic stations. Permanent stations (MULG, AS31, WRAB) indicated by
564 thicker circles. Grey bands in the upper plot represent the 140°-160° back-azimuthal
565 range at which most available events occur (see Figure 5), modulated by 90°. Stations
566 with fast directions that coincide with these grey bands would therefore in theory be
567 prone to generate nulls for such events.

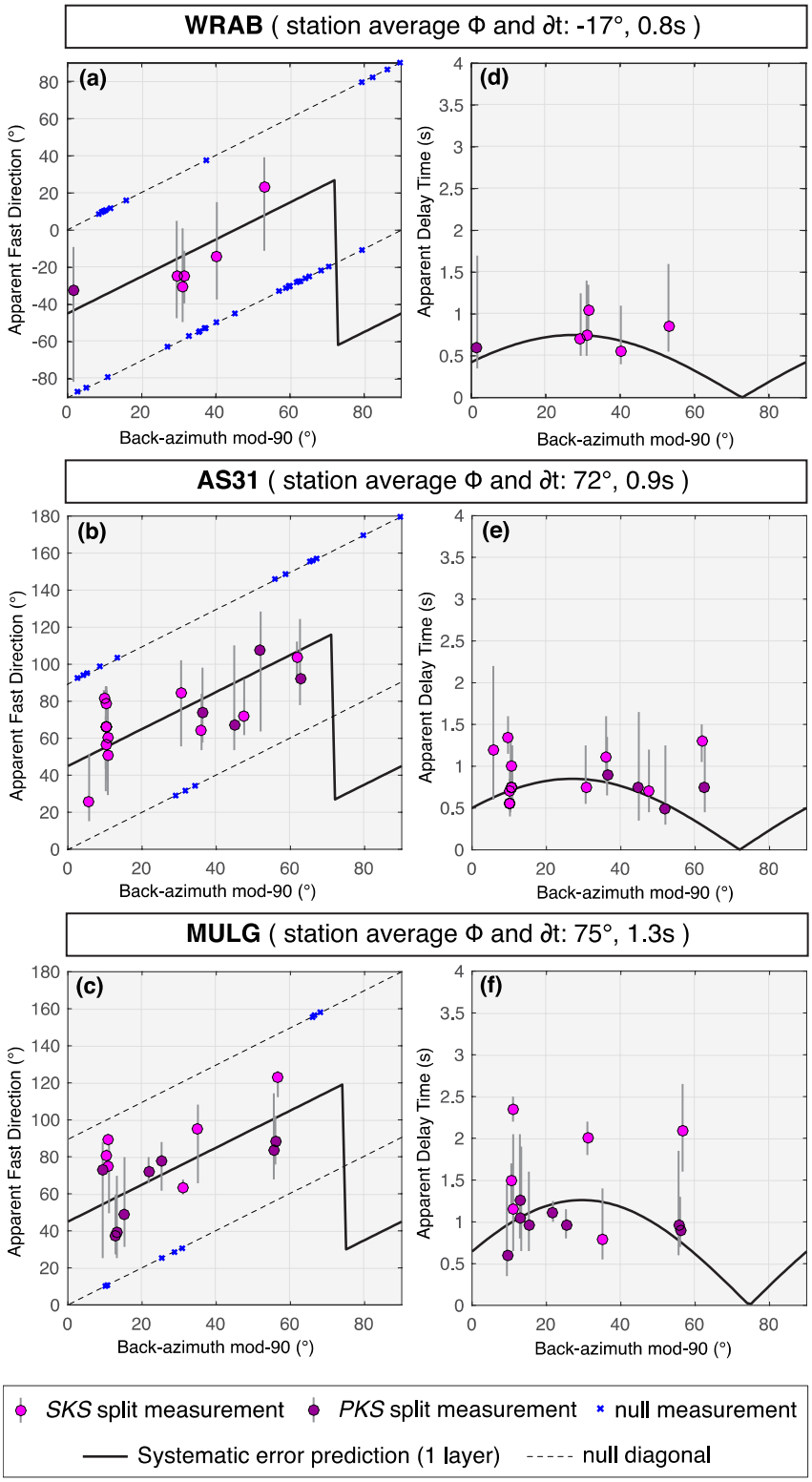
568



569

570 **Figure 5**. Histograms of the number of available event-station pairs (grey), null (blue)
571 and split (red) measurements made at BILBY stations according to event back-
572 azimuth. The majority of both null and split results are found in the back-azimuthal
573 range 140°-160°, corresponding to a peak in the number of available events in same
574 range.

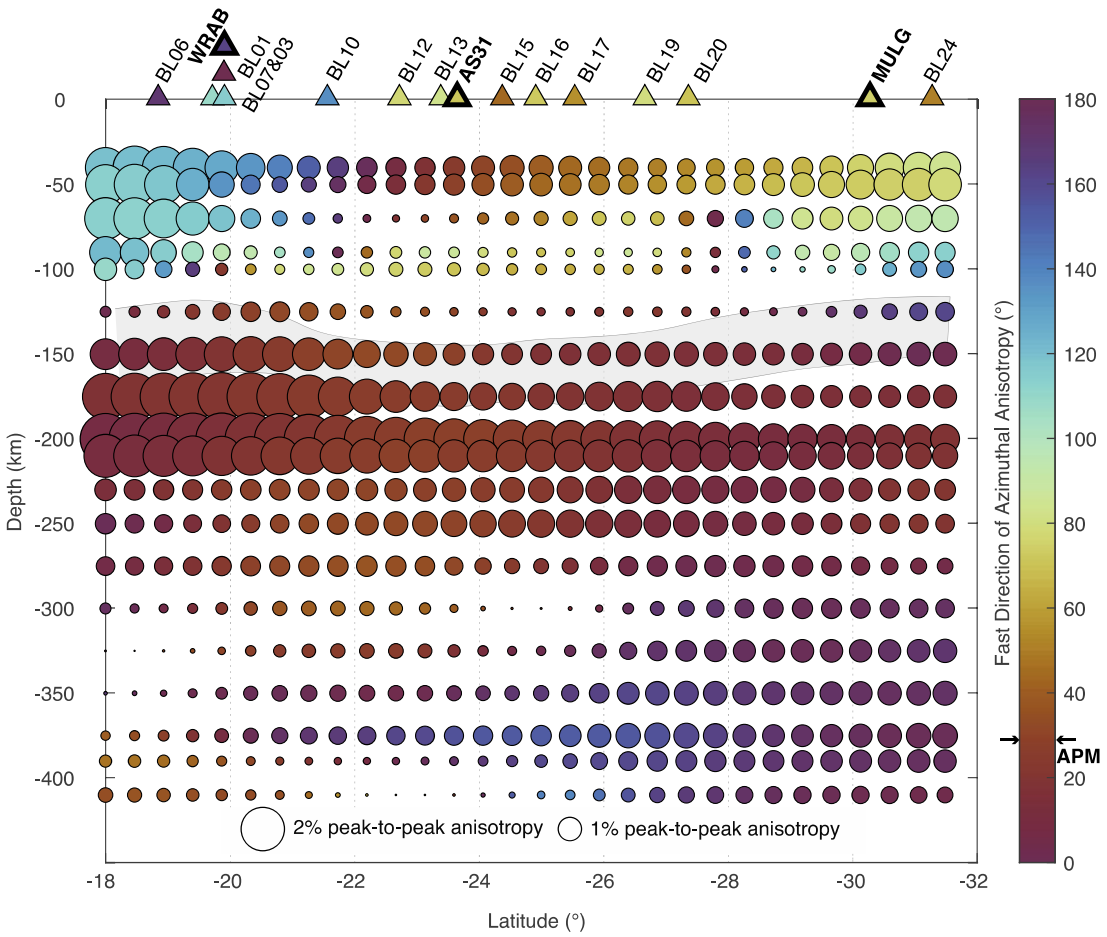
575



576

577 **Figure 6**. Variation in splitting parameters (Φ and δt) with respect to back-azimuth.
578 For the three permanent stations (WRAB, AS31, MULG) *SKS* and *PKS* splitting
579 results are plotted (magenta/purple dots with grey error bars) showing fast direction
580 (a-c) and delay time (d-f) as a function of event back-azimuth modulated over 90°.

For all stations the fast directions (a-c) follow a 45° slope, and conform to the predicted sawtooth pattern of systematic error (solid black line) expected for a single layer with the station average Φ and δt (Wüstefeld and Bokelmann, 2007), and calculated from equations 1 and 2 of Eakin et al. (2019). The thin dashed lines with the same 45° slope indicate where null measurements (blue crosses) plot (i.e. the null diagonal), when the fast direction equals the back-azimuth ±90°.



588

589 **Figure 7**. Cross-section of upper mantle S-wave azimuthal anisotropy beneath
590 BILBY along a N-S profile at 134° longitude. Rayleigh-wave derived azimuthal
591 anisotropy from Debayle et al. (2016) is represented by the grid of coloured circles.
592 The various colours indicate the fast direction of the tomographic model at that depth
593 according to the colour scale shown on the right. The size of the circle corresponds to
594 the strength of the anisotropy according to the scale shown at the bottom. For
595 comparison, at the top of the figure, the station averaged fast directions are included
596 as triangles coloured according to the same colour scale. The three permanent stations
597 are highlighted by outlining the triangles in bold black. The grey undulating band in
598 the background around 150 km corresponds to the depth of the lithosphere-
599 asthenosphere transition (LAT) beneath the BILBY profile estimated from radial
600 anisotropy and receiver function studies (Kennett and Sippl, 2018; Yoshizawa, 2014;
601 Yoshizawa and Kennett, 2015). On the colour-scale, the angle of absolute plate
602 motion (APM) beneath central Australia (~28° clockwise from north) is indicated by
603 the two black arrows (Kreemer et al., 2014).

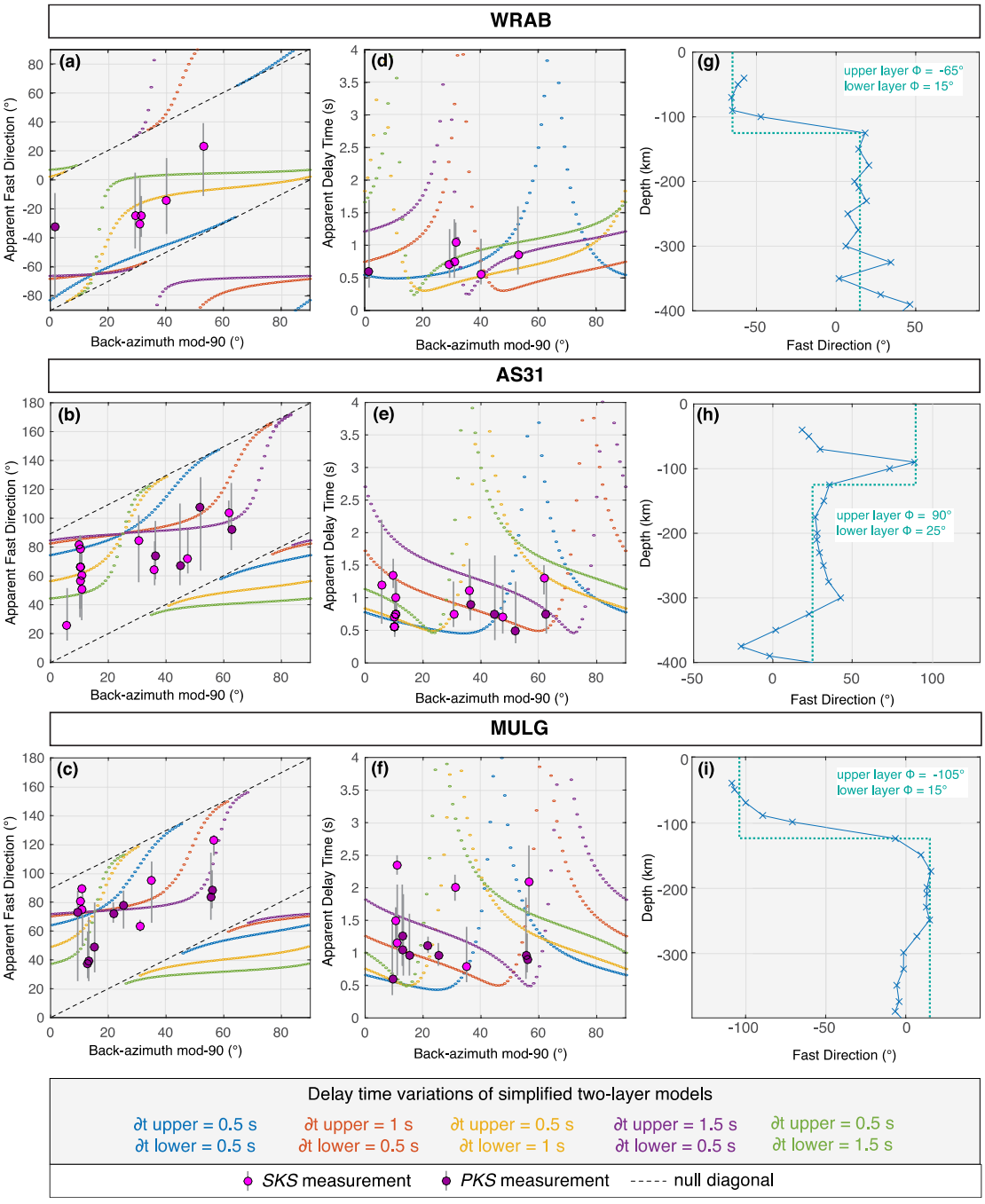
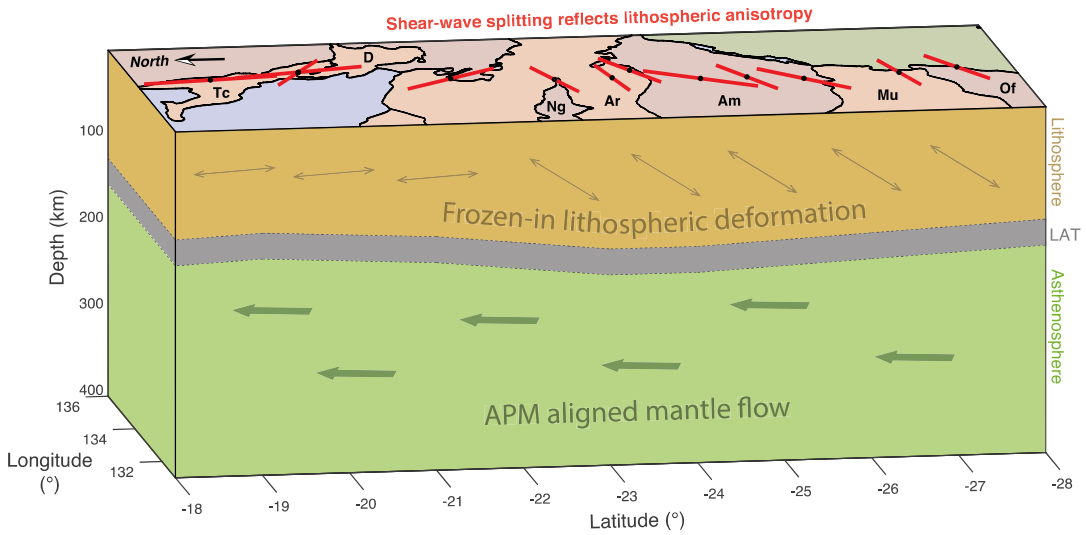


Figure 8. Modelling back-azimuthal variation in splitting parameters (Φ and δt) with simplified two-layer models for the three permanent stations (WRAB, AS31, MULG). Two-layer model predictions (small coloured circles; a-f) are plotted based on the general anisotropic structure beneath each station as suggested by surface-wave studies of azimuthal anisotropy (Debayle et al., 2016) (blue line; g-i). The fast direction in an upper lithospheric layer and a lower asthenospheric layer is approximated by the dotted turquoise line (g-i). The delay time attributed to each

612 layer is varied in 0.5 second increments, with the contributions of 5 different models
613 represented by the five different dotted curves (blue, red, yellow, purple, and green).

614



615

616 **Figure 9**. Schematic illustration showing our preferred interpretation of upper mantle
617 deformation and seismic anisotropy beneath central Australia. The pattern of shear-
618 wave splitting recorded at BILBY stations appears to primarily reflect past
619 deformation of the crust and lithosphere which has been preserved as anisotropy. LAT
620 = lithosphere-asthenosphere transition, same as Figure 7. APM = absolute plate
621 motion. Colours and abbreviations of geological regions same as Figure 1.

References

Aitken, A.R.A., 2010. Moho geometry gravity inversion experiment (MoGGIE): A refined model of the Australian Moho, and its tectonic and isostatic implications. Earth Planet. Sci. Lett. 297, 71–83. doi:10.1016/j.epsl.2010.06.004

Aitken, A.R.A., Betts, P.G., Ailleres, L., 2009a. The architecture, kinematics, and lithospheric processes of a compressional intraplate orogen occurring under Gondwana assembly: The Petermann orogeny, central Australia. Lithosphere 1, 343–357. doi:10.1130/L39.1

Aitken, A.R.A., Betts, P.G., Weinberg, R.F., Gray, D., 2009b. Constrained potential field modeling of the crustal architecture of the Musgrave Province in central Australia: Evidence for lithospheric strengthening due to crust-mantle boundary uplift. J. Geophys. Res. Solid Earth 114. doi:10.1029/2008JB006194

Amante, C., Eakins, B.W., 2009. ETOPO1 1 arc-minute global relief model: procedures, data sources and analysis. NOAA Tech. Memo. NESDIS NGDC-24 19.

Aragon, J.C., Long, M.D., Benoit, M.H., 2017. Lateral Variations in *SKS* Splitting Across the MAGIC Array, Central Appalachians. Geochemistry, Geophys. Geosystems 18, 4136–4155. doi:10.1002/2017GC007169

Bacchin, M., 2010. Gravity Anomaly Grid of the Australian Region - 2010. doi:http://pid.geoscience.gov.au/dataset/ga/70998

Bacchin, M., Milligan, P.R., Wynne, P., Tracey, R., 2008. Gravity anomaly map of the Australian region (Third Edition), scale 1:5000000. doi:http://pid.geoscience.gov.au/dataset/ga/65682

Bastow, I.D., Owens, T.J., Helffrich, G., Knapp, J.H., 2007. Spatial and temporal constraints on sources of seismic anisotropy: Evidence from the Scottish highlands. Geophys. Res. Lett. 34, 5305. doi:10.1029/2006GL028911

Bello, M., Cornwell, D.G., Rawlinson, N., Reading, A.M., 2019. Insights into the structure and dynamics of the upper mantle beneath Bass Strait, southeast Australia, using shear wave splitting. Phys. Earth Planet. Inter. 289, 45–62. doi:10.1016/J.PEPI.2019.02.002

Betts, P.G., Giles, D., 2006. The 1800-1100 Ma tectonic evolution of Australia. Precambrian Res. 144, 92–125. doi:10.1016/j.precamres.2005.11.006

Bird, P., 2003. An updated digital model of plate boundaries. Geochemistry, Geophys. Geosystems 4, 1027. doi:10.1029/2001GC000252

Blake, D.H., Kilgour, B., 1998. Geological Regions of Australia, 1:5 000 000 scale. doi:http://pid.geoscience.gov.au/dataset/ga/32366

Bowman, J.R., Ando, M., 1987. Shear-wave splitting in the upper-mantle wedge above the Tonga subduction zone. Geophys. J. Int. 88, 25–41. doi:10.1111/j.1365-246X.1987.tb01367.x

Chen, X., Levin, V., Yuan, H., 2021. Small Shear Wave Splitting Delays Suggest Weak Anisotropy in Cratonic Mantle Lithosphere. Geophys. Res. Lett. e2021GL093861. doi:10.1029/2021GL093861

Clitheroe, G., van der Hilst, R., 1998. Complex Anisotropy in the Australian Lithosphere from Shear-wave Splitting in Broad-band SKS Records. Geodyn. Ser. 26, 73–78. doi:10.1002/9781118670095.ch5

Conrad, C.P., Behn, M.D., Silver, P.G., 2007. Global mantle flow and the development of seismic anisotropy: Differences between the oceanic and continental upper mantle. J. Geophys. Res. 112, B07317. doi:10.1029/2006JB004608

671 Crameri, F., Shephard, G.E., Heron, P.J., 2020. The misuse of colour in science
672 communication. Nat. Commun. 11, 5444. doi:10.1038/s41467-020-19160-7
673 Crampin, S., 1994. The fracture criticality of crustal rocks. Geophys. J. Int. 118, 428–
674 438. doi:10.1111/j.1365-246X.1994.tb03974.x
675 Debayle, E., Dubuffet, F., Durand, S., 2016. An automatically updated S -wave model
676 of the upper mantle and the depth extent of azimuthal anisotropy. Geophys. Res.
677 Lett. 43, 674–682. doi:10.1002/2015GL067329
678 Debayle, E., Kennett, B., Priestley, K., 2005. Global azimuthal seismic anisotropy and
679 the unique plate-motion deformation of Australia. Nature 433, 509–512.
680 doi:10.1038/nature03247
681 Debayle, E., Ricard, Y., 2013. Seismic observations of large-scale deformation at the
682 bottom of fast-moving plates. Earth Planet. Sci. Lett. 376, 165–177.
683 doi:10.1016/j.epsl.2013.06.025
684 Djomani Poudjom, Y., Minty, B.R.S., Hutchens, M., Lane, R.J.L., 2019. Total
685 Magnetic Intensity (TMI) Grid of Australia 2019 - seventh edition - 80 m cell
686 size. doi:http://dx.doi.org/10.26186/5e9cf3f2c0f1d
687 Eakin, C.M., 2021. Quasi-Love wave scattering reveals tectonic history of Australia
688 and its margins reflected by mantle anisotropy. Commun. Earth Environ. In
689 Press.
690 Eakin, C.M., Long, M.D., 2013. Complex anisotropy beneath the Peruvian flat slab
691 from frequency-dependent, multiple-phase shear wave splitting analysis. J.
692 Geophys. Res. Solid Earth 118, 4794–4813. doi:10.1002/jgrb.50349
693 Eakin, C.M., Long, M.D., Wagner, L.S., Beck, S.L., Tavera, H., 2015. Upper mantle
694 anisotropy beneath Peru from SKS splitting: Constraints on flat slab dynamics
695 and interaction with the Nazca Ridge. Earth Planet. Sci. Lett. 412, 152–162.
696 doi:10.1016/j.epsl.2014.12.015
697 Eakin, C.M., Obrebski, M., Allen, R.M., Boyarko, D.C., Brudzinski, M.R., Porritt, R.,
698 2010. Seismic anisotropy beneath Cascadia and the Mendocino triple junction:
699 Interaction of the subducting slab with mantle flow. Earth Planet. Sci. Lett. 297,
700 627–632. doi:10.1016/j.epsl.2010.07.015
701 Eakin, C.M., Rychert, C.A., Harmon, N., 2018. The Role of Oceanic Transform
702 Faults in Seafloor Spreading: A Global Perspective From Seismic Anisotropy. J.
703 Geophys. Res. Solid Earth 123, 1736–1751. doi:10.1002/2017JB015176
704 Eakin, C.M., Wirth, E.A., Wallace, A., Ulberg, C.W., Creager, K.C., Abers, G.A.,
705 2019. SKS Splitting Beneath Mount St. Helens: Constraints on Subslab Mantle
706 Entrainment. Geochemistry, Geophys. Geosystems 20.
707 doi:10.1029/2019GC008433
708 Fichtner, A., Kennett, B.L.N., Igel, H., Bunge, H.P., 2010. Full waveform
709 tomography for radially anisotropic structure: New insights into present and past
710 states of the Australasian upper mantle. Earth Planet. Sci. Lett. 290, 270–280.
711 doi:10.1016/j.epsl.2009.12.003
712 Fichtner, A., Kennett, B.L.N., Igel, H., Bunge, H.P., 2009. Full seismic waveform
713 tomography for upper-mantle structure in the Australasian region using adjoint
714 methods. Geophys. J. Int. 179, 1703–1725. doi:10.1111/j.1365-
715 246X.2009.04368.x
716 Fishwick, S., Reading, A.M., 2008. Anomalous lithosphere beneath the Proterozoic of
717 western and central Australia: A record of continental collision and intraplate
718 deformation? Precambrian Res. 166, 111–121.
719 doi:10.1016/j.precamres.2007.04.026
720 Ford, H.A., Fischer, K.M., Abt, D.L., Rychert, C.A., Elkins-Tanton, L.T., 2010. The

lithosphere–asthenosphere boundary and cratonic lithospheric layering beneath Australia from Sp wave imaging. Earth Planet. Sci. Lett. 300, 299–310. doi:10.1016/j.epsl.2010.10.007

Fouch, M.J., Rondenay, S., 2006. Seismic anisotropy beneath stable continental interiors. Phys. Earth Planet. Inter. 158, 292–320. doi:10.1016/j.pepi.2006.03.024

Goleby, B.R., Shaw, R.D., Wright, C., Kennett, B.L.N., Lambeck, K., 1989. Geophysical evidence for "thick-skinned" crustal deformation in central Australia. Nature 337, 325–330. doi:10.1038/337325a0

Haines, P.W., Hand, M., Sandiford, M., 2001. Palaeozoic synorogenic sedimentation in Central and Northern Australia: A review of distribution and timing with implications for the evolution of intracontinental orogens. Aust. J. Earth Sci. 48, 911–928. doi:10.1046/j.1440-0952.2001.00909.x

Heintz, M., Kennett, B.L.N., 2006. The apparently isotropic Australian upper mantle. Geophys. Res. Lett. 33, L15319. doi:10.1029/2006GL026401

Heintz, M., Kennett, B.L.N., 2005. Continental scale shear wave splitting analysis: Investigation of seismic anisotropy underneath the Australian continent. Earth Planet. Sci. Lett. 236, 106–119. doi:10.1016/j.epsl.2005.05.003

Helffrich, G., Silver, P., Given, H., 1994. Shear-wave splitting variation over short spatial scales on continents. Geophys. J. Int. 119, 561–573. doi:10.1111/j.1365-246X.1994.tb00142.x

Ismaïl, W. Ben, Mainprice, D., 1998. An olivine fabric database: An overview of upper mantle fabrics and seismic anisotropy. Tectonophysics 296, 145–157. doi:10.1016/S0040-1951(98)00141-3

Karato, S., Jung, H., Katayama, I., Skemer, P., 2008. Geodynamic Significance of Seismic Anisotropy of the Upper Mantle: New Insights from Laboratory Studies. Annu. Rev. Earth Planet. Sci. 36, 59–95. doi:10.1146/annurev.earth.36.031207.124120

Kendall, J.M., Silver, P.G., 1996. Constraints from seismic anisotropy on the nature of the lowermost mantle. Nature 381, 409–412. doi:10.1038/381409a0

Kennett, B.L.N., Iaffaldano, G., 2013. Role of lithosphere in intra-continental deformation: Central Australia. Gondwana Res. 24, 958–968. doi:10.1016/j.gr.2012.10.010

Kennett, B.L.N., Sippl, C., 2018. Lithospheric discontinuities in Central Australia. Tectonophysics 744, 10–22. doi:10.1016/j.tecto.2018.06.008

Kreemer, C., Blewitt, G., Klein, E.C., 2014. A geodetic plate motion and Global Strain Rate Model. Geochemistry, Geophys. Geosystems 15, 3849–3889. doi:10.1002/2014GC005407

Lambeck, K., 1986. Crustal structure and evolution of the central Australian basins. Geol. Soc. London, Spec. Publ. 24, 133–145. doi:10.1144/GSL.SP.1986.024.01.13

Lambeck, K., 1983. Structure and evolution of the intracratonic basins of central Australia. Geophys. J. R. Astron. Soc. 74, 843–886. doi:10.1111/j.1365-246X.1983.tb01907.x

Lambeck, K., Burgess, G., 1992. Deep crustal structure of the musgrave block, central australia: Results from teleseismic travel-time anomalies. Aust. J. Earth Sci. 39, 1–19. doi:10.1080/08120099208727996

Liu, J., Wu, J., Wang, W., Fang, L., Chang, K., 2020. Seismic anisotropy beneath the eastern margin of the Tibetan Plateau from SKS splitting observations. Tectonophysics 785, 228430. doi:10.1016/j.tecto.2020.228430

771 Long, M.D., Becker, T.W., 2010. Mantle dynamics and seismic anisotropy. Earth
772 Planet. Sci. Lett. 297, 341–354. doi:10.1016/j.epsl.2010.06.036
773 Monteiller, V., Chevrot, S., 2010. How to make robust splitting measurements for
774 single-station analysis and three-dimensional imaging of seismic anisotropy.
775 Geophys. J. Int. 182. doi:10.1111/j.1365-246X.2010.04608.x
776 Myers, J.S., Shaw, R.D., Tyler, I.M., 1996. Tectonic evolution of Proterozoic
777 Australia. TECTONICS 15, 1431–1446. doi:10.1029/96TC02356
778 Nicolas, A., Christensen, N.I., 1987. Formation of anisotropy in upper mantle
779 peridotites: A review, in: Fuchs, K., Froidevaux, C. (Eds.), Composition,
780 Structure and Dynamics of the Lithosphere-Asthenosphere System. American
781 Geophysical Union, pp. 111–123. doi:10.1029/GD016p0111
782 Özalaybey, S., Chen, W.P., 1999. Frequency-dependent analysis of SKS/SKKS
783 waveforms observed in Australia: Evidence for null birefringence. Phys. Earth
784 Planet. Inter. 114, 197–210. doi:10.1016/S0031-9201(99)00058-8
785 Rabbel, W., Mooney, W.D., 1996. Seismic anisotropy of the crystalline crust: what
786 does it tell us? Terra Nov. 8, 16–21. doi:10.1111/j.1365-3121.1996.tb00721.x
787 Rawlinson, S., Kennett, B.L.N., 2008. BILBY - Australian Cratonic Lithosphere.
788 doi:10.7914/SN/6F_2008
789 Saltzer, R.L., Gaherty, J.B., Jordan, T.H., 2000. How are vertical shear wave splitting
790 measurements affected by variations in the orientation of azimuthal anisotropy
791 with depth? Geophys. J. Int. 141, 374–390. doi:10.1046/j.1365-
792 246x.2000.00088.x
793 Silver, P., Chan, W., 1988. Implications for continental structure and evolution from
794 seismic anisotropy. Nature 335, 34–39. doi:10.1038/335034a0
795 Silver, P.G., 1996. SEISMIC ANISOTROPY BENEATH THE CONTINENTS:
796 Probing the Depths of Geology. Annu. Rev. Earth Planet. Sci. 24, 385–432.
797 doi:10.1146/annurev.earth.24.1.385
798 Silver, P.G., Chan, W.W., 1991. Shear Wave Splitting and Sub continental Mantle
799 Deformation. J. Geophys. Res. Solid Earth 96, 16429–16454.
800 doi:10.1029/91JB00899
801 Silver, P.G., Gao, S.S., Liu, K.H., 2001. Mantle deformation beneath southern Africa.
802 Geophys. Res. Lett. 28, 2493–2496. doi:10.1029/2000GL012696
803 Silver, P.G., Savage, M.K., 1994. The Interpretation of Shear-Wave Splitting
804 Parameters In the Presence of Two Anisotropic Layers. Geophys. J. Int. 119,
805 949–963. doi:10.1111/j.1365-246X.1994.tb04027.x
806 Simons, F.J., van der Hilst, R.D., 2003. Seismic and mechanical anisotropy and the
807 past and present deformation of the Australian lithosphere. Earth Planet. Sci. Lett.
808 211, 271–286. doi:10.1016/S0012-821X(03)00198-5
809 Simons, F.J., van der Hilst, R.D., Montagner, J.P., Zielhuis, A., 2002. Multimode
810 Rayleigh wave inversion for heterogeneity and azimuthal anisotropy of the
811 Australian upper mantle. Geophys. J. Int. 151, 738–754. doi:10.1046/j.1365-
812 246X.2002.01787.x
813 Sippl, C., 2016. Moho geometry along a north-south passive seismic transect through
814 Central Australia. Tectonophysics 676, 56–69. doi:10.1016/j.tecto.2016.03.031
815 Vauchez, A., Tommasi, A., Barruol, G., 1998. Rheological heterogeneity, mechanical
816 anisotropy and deformation of the continental lithosphere. Tectonophysics 296,
817 61–86. doi:10.1016/S0040-1951(98)00137-1
818 Vecsey, L., Plomerová, J., Babuška, V., 2008. Shear-wave splitting measurements —
819 Problems and solutions. Tectonophysics 462, 178–196.
820 doi:10.1016/J.TECTO.2008.01.021

Walter, M.R., Veevers, J.J., Calver, C.R., Grey, K., 1995. Neoproterozoic stratigraphy of the Centralian Superbasin, Australia. Precambrian Res. 73, 173–195. doi:10.1016/0301-9268(94)00077-5

Wellman, P., 1976. Gravity trends and the growth of australia: A tentative correlation. J. Geol. Soc. Aust. 23, 11–14. doi:10.1080/00167617608728917

Wüstefeld, A., Bokelmann, G., 2007. Null Detection in Shear-Wave Splitting Measurements. Bull. Seismol. Soc. Am. 97, 1204–1211. doi:10.1785/0120060190

Wüstefeld, A., Bokelmann, G., Zaroli, C., Barruol, G., 2008. SplitLab: A shear-wave splitting environment in Matlab. Comput. Geosci. 34, 515–528. doi:10.1016/j.cageo.2007.08.002

Yoshizawa, K., 2014. Radially anisotropic 3-D shear wave structure of the Australian lithosphere and asthenosphere from multi-mode surface waves. Phys. Earth Planet. Inter. 235, 33–48. doi:10.1016/j.pepi.2014.07.008

Yoshizawa, K., Kennett, B.L.N., 2015. The lithosphere-asthenosphere transition and radial anisotropy beneath the Australian continent. Geophys. Res. Lett. 42, 3839–3846. doi:10.1002/2015GL063845

Zhao, G., Cawood, P.A., Wilde, S.A., Sun, M., 2002. Review of global 2.1-1.8 Ga orogens: Implications for a pre-Rodinia supercontinent. Earth-Science Rev. 59, 125–162. doi:10.1016/S0012-8252(02)00073-9